INFLUENCE OF Mn AND S ON THE PROPERTIES OF CAST IRON PART III– TESTING AND ANALYSIS

Richard Gundlach
Element Materials Technology, Wixom, MI, USA

Matthew Meyer
Kohler Co., Kohler, WI, USA

Leonard Winardi
Charlotte Pipe, Charlotte, NC, USA

Abstract

This work is the culmination of a literature review and foundry experiments designed to re-examine the roles of Mn and S on the strength of gray iron.

A review of the literature showed that there are two principal regions in gray iron chemistries. A region where Mn and S levels are below the solubility limit of MnS at the solidification temperature, and a region above the solubility limit. Twenty-four heats were produced in cast sections up to 3 inches to investigate the influence of S on strength at three Mn levels, including low S concentrations, where S is fully soluble and no MnS precipitation occurs before the start of eutectic solidification. At each Mn level, S was progressively increased until MnS precipitated in the melt prior to reaching the eutectic temperature.

Master heats were produced at three Mn levels (0.3%, 0.5% and 0.8%). Sulfur was varied from 0.01% to 0.15%. The base chemistry was otherwise typical of Class 35 gray iron at a carbon equivalent (CE) value of 3.9 to 4.0 and sufficient alloying with Cu and Sn to assure a fully pearlitic structure. Tensile strength, hardness, chill width, and thermal arrests were determined.

Tensile strength first increased with sulfur, reaching a maximum strength level, and then decreased with further increases in sulfur. Maximum strength coincided with the solubility limit of MnS inclusions. Strengths reached 42 ksi in the 1.2 inch B test bar, and 36 ksi in the 3 inch diameter test bar. For each Mn series, the differences in strength between maximum and minimum values were 44% and 38% for the B test bars and 3 inch bars, respectively. Variations in chilling tendency were modest, except at the extreme lowest and highest S levels.

Keywords: *gray iron, cast iron, Mn:S ratio, MnS solubility, free sulfur, tensile strength, chill, thermal analysis, cell count*

Introduction

Sulfur is generally considered a tramp element in cast iron, and its level must be controlled.[1-4] When manganese is not present at sufficient concentrations, sulfur reacts with iron to produce a low-melting phase (FeS) that may produce hot-shortness. Sulfur is a surface active element that can exhibit many negative effects, including the promotion of degenerate graphite forms, intercellular carbides, increased chilling tendency and high hardness pearlite. Sulfur combines with manganese in the iron to form MnS, and it is necessary that Mn be present to tie up S and avoid the undesirable consequences of elevated S. Consequently, industry has always added Mn to control S.

The literature suggests that Mn should be present at levels approaching the stoichiometric ratio (Mn:S = 1.7:1) to avoid the negative influence of sulfur. More than 80 years ago Norbury[1] recommended that the Mn concentration should be in excess of the stoichiometric ratio (Mn:S = 1.7:1) to avoid FeS formation. He proposed that Mn levels should be 0.30% in excess of 1.7 times %S. His proposal was widely accepted and, to the present day, it has been employed almost universally in the production of gray cast iron. More recently, Mampaey[2] offered a refinement to this formula, recommending an excess Mn of 0.2 to 0.3% for irons with 0.1%S or less, and an excess Mn of 0.4 to 0.5% for irons with greater than 0.1%S. Others have recommended controlling the Mn:S ratio in the range of 2 to 7.

The findings of the literature review associated with this study, Part I – Historical Perspective,[5] also showed that sulfur produces positive benefits, including increased cell count, improved response to inoculation and increased strength. Researchers showed that as S increased, the tensile properties improved up to a peak level, and then began to de-

crease with further increases in S or Mn. The data of several investigations showed that substantial decreases in strength occurred, when cast irons are produced at compositions that are well in excess of the solubility limit of MnS. While no researchers plotted mechanical properties against the product of %Mn and %S, when re-plotting the published data, a correlation of peak strength with solubility limit of MnS was found. The fall off in strength generally occurred when %Mn x %S exceeded a value around 0.03.

The reader is reminded that the solubility of S and MnS are a function of %Mn x %S and temperature. Thus, the solubility of S decreases with increasing Mn and decreasing temperature. In Part I,[5] we show that the solubility limit occurs when %Mn x %S exceeds a value between 0.030 and 0.045. The exact value depends on the carbon equivalent of the iron. If the MnS concentration is above the solubility limit of the iron, MnS will precipitate from the melt prior to reaching the eutectic temperature.

Consequently, the role of Mn is two-fold: (1) it reacts with S to produce MnS inclusions, and equally important, (2) it influences the dissolved or free S content of the iron when eutectic solidification takes place. The free energy of formation for MnS is low and, thus, the equilibrium constant is relatively high. Therefore, there is always some free S still dissolved in the liquid metal when it reaches the eutectic temperature, and the free sulfur exhibits a strong influence on the microstructure and various properties of cast iron.

In summary, the data from the literature appears to show that there are two competing reactions taking place in gray cast iron. At lower Mn and S concentrations, no MnS precipitates from the melt prior to eutectic solidification, and mechanical properties increase with increasing sulfur content. At higher concentrations, MnS will precipitate from the melt ahead of eutectic solidification. When MnS inclusions form, they appear to change the relationship between dissolved S and strength. Maximum strength appears to occur when the MnS solubility limit is reached. At concentrations above the solubility limit, strength falls off with further increases in S or Mn.

It is proposed that a better way to balance Mn and S in cast iron is to adjust the Mn and S levels according to the equilibrium constant, that is, the product of %Mn x %S. Mn and S should be present at levels that meet or just exceed the solubility limit at the eutectic temperature of the alloy. And, maximum strength is achieved when the composition coincides with this equilibrium constant value. The results of the literature review[5] are the basis for this research project which aims to improve our understanding of how to balance Mn and S in cast iron.

An intensive production-scale experiment was designed to investigate the influence of S on strength at lower Mn concentrations, where MnS precipitation occurs only after the start of eutectic solidification, and to address both the regions above and below the solubility limit of MnS. The manufacture of test castings for this study is described in Part II - Experimental Design: Aspects of Melting and Pouring.[6]

From one master heat of carefully selected charge materials, cast iron alloys of three Mn concentrations (nominally 0.3%, 0.5% and 0.8%) were produced. From each master alloy, eight split heats were poured with sulfur contents ranging from nominally 0.01% to 0.15%. Each of the split heats were poured into green sand test molds produced on an automated match plate molding machine containing horizontally-cast test bars with a wide range of section sizes ranging from 0.88 to 3.0 inches in diameter, including ASTM A48 A, B and C test bar designations. In addition, ASTM A367 W2 chill wedges and thermal analysis cups were poured.

The base composition of the master heat was typical of a Class 35 gray iron with a CE value of 3.9 to 4.0. The master heat was modestly alloyed with 0.3%Cu and 0.04%Sn to assure that a fully pearlitic matrix microstructure would be attained in all test bars. Ladle inoculation was performed with 0.25% ferrosilicon.

For the analysis, the castings were sectioned to obtain various test specimens. Subsequently, chemistry, hardness and tensile strength were determined. The graphite structures were evaluated for graphite type, flake size and flake count. Eutectic cell size was determined for some test bars. Chill width was measured and thermal analysis was performed.

Procedures and Results

A bar length of 6 inches was cut from the A and B test bars for obtaining machining blanks for the tensile test specimens. For the C test bars and the 3 inch diameter test bars, blanks were cut from a mid-radius position. Metallographic samples were excised from the gauge section of the broken tensile specimens. After sectioning, hardness was determined on the outer cast surface of the A and B test bars, and from the saw-cut surface of the machining blanks from the C test bars and 3 inch bars. Chemistry was performed on the spectrometer buttons that were sampled from the pouring ladles.

Chemical Analysis

Chemical analysis had been performed by Bremen Castings Inc and the results were reported in Part II. The analysis of several split heats was also performed. The spectrometer buttons and companion pin samples were analyzed. Carbon and sulfur were determined from the chilled pin samples using combustion methods. The remaining elements were determined by Glow Discharge Spectrometry. The results of chemical analysis are reported in Table 1.

Table 1. Results of Chemical Analysis in wt-%

Element	0.28% Mn series			0.47% Mn series			0.78% Mn series		
Ladle #	1	4	8	9	12	16	17	20	24
S	0.005	0.044	0.15	0.030	0.051	0.13	0.031	0.043	0.15
CE	4.03	4.02	3.97	3.94	3.99	3.95	3.91	3.89	3.83
C	3.32	3.34	3.32	3.27	3.30	3.27	3.25	3.19	3.17
P	0.029	0.027	0.028	0.028	0.028	0.028	0.029	0.029	0.028
Si	2.10	2.02	1.91	1.99	2.04	2.02	1.96	2.06	1.95
Mn	0.28	0.28	0.27	0.46	0.47	0.46	0.78	0.83	0.78
Cr	0.05	0.05	0.05	0.05	0.05	0.05	0.05	0.05	0.05
Cu	0.33	0.33	0.33	0.33	0.33	0.32	0.33	0.33	0.32
Ni	0.06	0.05	0.05	0.06	0.06	0.06	0.06	0.06	0.06
Mo	<0.01	<0.01	<0.01	<0.01	<0.01	<0.01	<0.01	<0.01	<0.01
V	0.018	0.019	0.019	0.018	0.019	0.019	0.018	0.020	0.021
Al	0.009	0.020	0.043	0.011	0.020	0.040	0.005	0.017	0.028
Ti	0.012	0.010	0.011	0.010	0.011	0.011	0.010	0.011	0.010
Sb	<0.005	<0.005	<0.005	<0.005	<0.005	<0.005	<0.005	<0.005	<0.005
Sn	0.048	0.044	0.047	0.045	0.044	0.047	0.043	0.044	0.037

Table 2. Results of Mechanical Testing

Series ID	% Sulfur	A Bar		B Bar		C Bar		3" Bar	
		UTS, ksi	HB	UTS, ksi	HB	UTS, ksi	HB	UTS, ksi	HB
0.28% Mn Series									
	0.005	41.2 37.2	208	32.2 33.1	185	28.7	174	29.1	170
	0.017	43.8 44.0	211	37.6 37.5	192	32.4	176	32.8	179
	0.026	44.7 43.6	212	35.4 37.4	196	33.9	181	33.0	178
	0.044	45.2 42.8	220	37.5 38.6	198	33.2	178	33.5	186
	0.062	42.9	218	37.2 37.9	201	33.4	203	30.1	178
	0.087	34.3 41.4	232	35.0 35.4	207	29.3	184	28.4	177
	0.10	32.9 18.5	235	33.3 33.6	209	25.8	187	29.0	183
	0.15	26.5 28.5	232	26.8 31.5	218	27.8	209	28.3	199
0.47% Mn Series									
	0.030	46.0 48.4	214	40.6 40.3	197	34.8	199	33.9	187
	0.020	43.2 43.5	206	37.5 38.1	196	34.8	201	34.3	184
	0.027	46.4 44.3	218	37.6 39.4	194	35.1	202	35.4	191
	0.051	43.1 42.3	208	36.2 36.5	200	33.0	182	33.0	184
	0.067	41.5 40.9	210	35.8 35.5	198	27.6	177	31.0	185
	0.085	41.6 44.1	239	35.0 35.4	201	28.1	189	25.6	179
	0.11	42.3 40.9	218	35.7 36.5	202	29.0	186	25.7	178
	0.13		221	33.4 41.3	207	26.2	188	26.6	187
0.78% Mn Series									
	0.031	43.8 45.3	215	39.1 39.5	202	32.4	190	32.7	198
	0.026	46.5 49.6	224	41.1 42.0	207	37.1	189	34.0	193
	0.026	49.3 49.4	227	40.5 39.9	199	31.5	191	34.7	192
	0.043	46.5 48.2	215	40.9 41.3	205	35.1	194	36.0	192
	0.060	45.1 45.1	217	39.8 40.3	203	35.5	193	34.8	191
	0.084	40.9	232	41.2 35.3	205	34.9	192	33.9	187
	0.11			39.2 38.6	205	29.5	189	29.2	194
	0.15		213	34.9 33.4	202	29.9	183	28.5	182

Hardness Testing

Brinell hardness was determined on the tensile blanks prior to machining the tensile specimens. A hardness measurement was determined for each bar size and each ladle. Hardness readings were performed using a computer-automated optical indentation reader, after hand-grinding to remove the cast surface and to make the surface flat and smooth. Hardness testing was performed in general accordance with ASTM Standard E10, using a 3000 kg load and 10 mm tungsten carbide ball indenter. The results of the hardness testing are listed in Table 2.

Tensile Testing

Tensile test specimens were machined from the A, B, C and 3 inch test bars. The specimens were machined with threaded grips and the gauge sections measured 0.5 inch diameter by 1.0 inch long for the A bars. For the B and C test bars and the 3 inch bars, the gauge sections measured 0.75 inch diameter by 1.0 inch long. The dimensions of the test bars conform to ASTM Standard E8. The test specimens were tested using a crosshead speed of 0.10 inch per minute until failure. A total of 144 tensile specimens were machined and tested. The tensile test results are presented in Table 2. The test results are plotted in Figures 1 through 3.

Microstructure Evaluation

Metallographic samples were obtained from the gauge sections of the broken tensile specimens. One specimen from each cast section for each of the 24 ladle chemistries was obtained for a total of 96 samples. The sectioning plane was parallel to the fracture face and approximately 6mm away from the fracture face. The samples were compression-mounted in Bakelite. The mounted specimens were ground using silicon carbide abrasives. The specimens were then polished by conventional mechanical methods using diamond abrasives and then final-polished with 0.05 µm colloidal silica.

The size and distribution of the graphite flakes were analyzed by automated image analysis. The analysis was performed on five fields at 50X magnification. Flake length was determined by measuring the feret distance between the tips of each flake. Type A graphite was predominant in the B bars, but the amount of type D graphite increased with sulfur content.

The specimens were subsequently etched in 4% picral and once more examined for matrix structure and the presence of hard micro constituents such as chill carbides, intercellular carbides and phosphides, and for sulfide distribution. As anticipated, the metallic matrix in all specimens was fully pearlitic. The specimens were also inspected for degenerate graphite forms resulting from elevated sulfur concentrations. Samples from every Mn series displayed degenerate flake forms at the higher sulfur concentrations (0.084% and above). Only samples from the 0.28% Mn series displayed intercellular carbides, which were observed at the highest sulfur concentrations. Representative photomicrographs displaying the "spiky" graphite and the intercellular carbides observed are shown in Figures 4 and 5.

The distribution of the manganese sulfide inclusions was evaluated in the as-polished specimens. At lower S con-

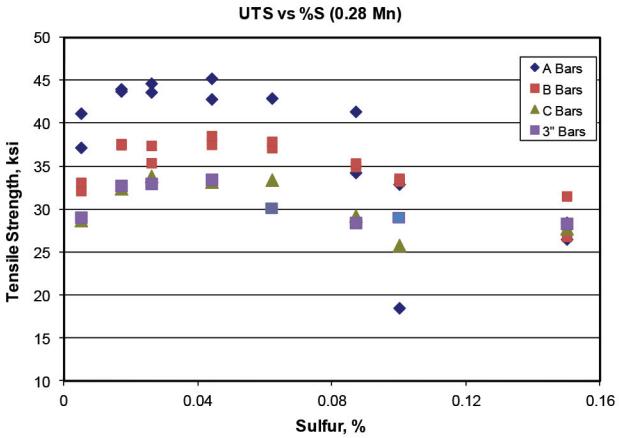

Figure 1. Tensile strength as a function of % sulfur in the 0.28%Mn series.

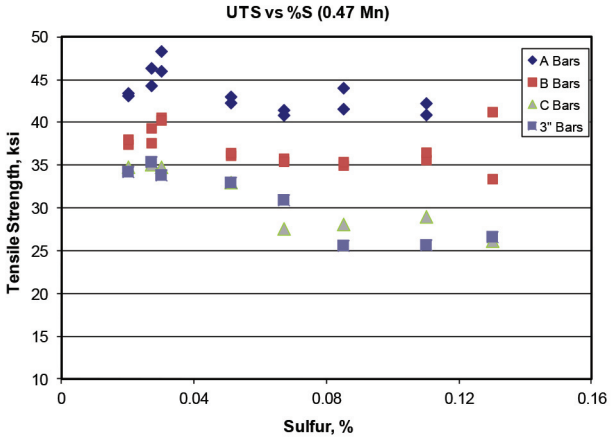

Figure 2. Tensile strength as a function of % sulfur in the 0.47%Mn series.

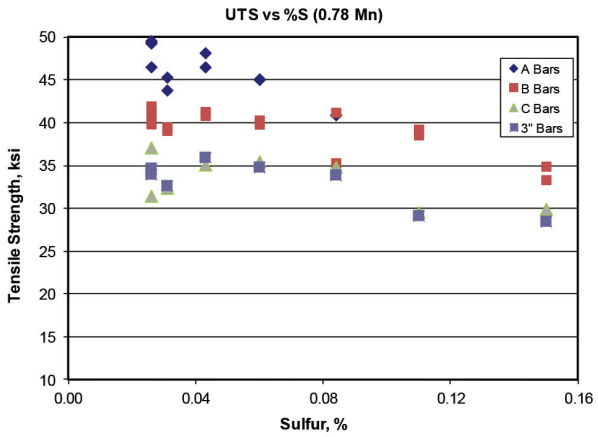

Figure 3. Tensile strength as a function of % sulfur in the 0.78%Mn series.

centrations, the MnS inclusions were concentrated between the secondary dendrite arms of the proeutectic dendrites. At higher combinations of Mn and S, the MnS inclusions were uniformly distributed. Micrographs illustrating the two types of MnS distributions are shown in Figures 6 and 7.

The flake graphite structures in the B test bars with maximum and minimum strength in each Mn series are shown in Figures 8 to 13.

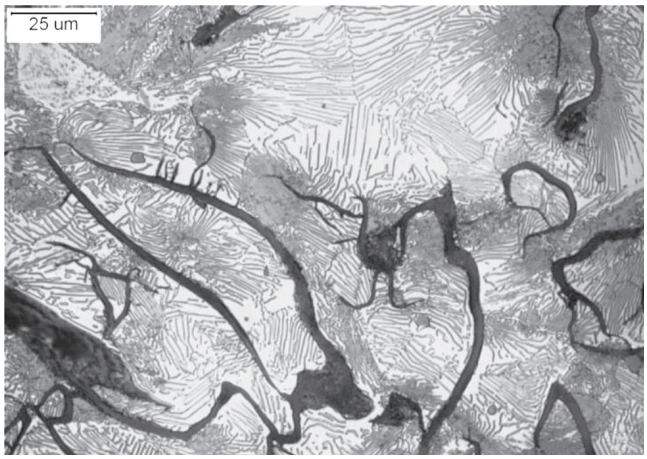

Figure 4. Spiky graphite in B-bar with 0.28%Mn and 0.087%S.

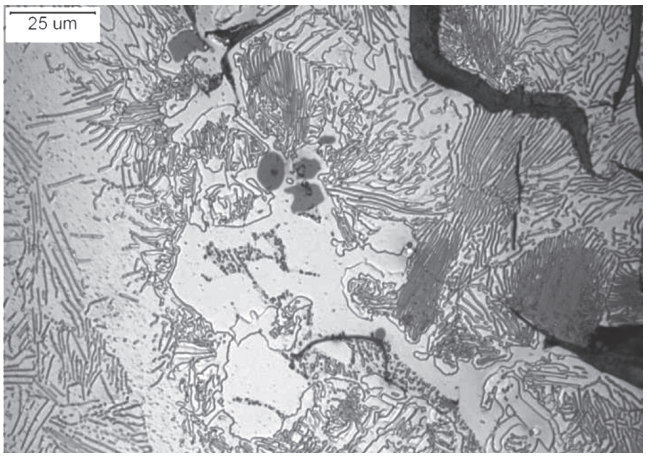

Figure 5. Intercellular carbides in C-bar with 0.28%Mn and 0.10%S.

Figure 6. Interdendritic distribution of MnS inclusions in B-bar with 0.28%Mn and 0.04%S.

Figure 7. Uniform distribution of MnS inclusions in B-bar with 0.78%Mn and 0.11%S.

Figure 8. Graphite structure in B-bar displaying highest strength (with 0.28%Mn and 0.02%S).

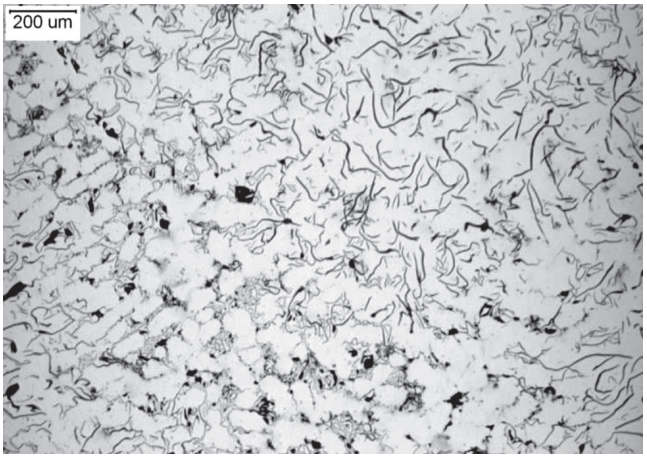

Figure 9. Graphite structure in B-bar displaying lowest strength (with 0.28%Mn and 0.15%S).

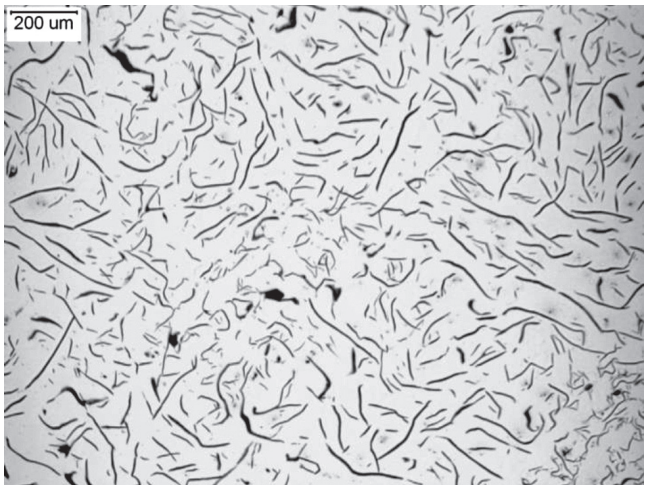

Figure 10. Graphite structure in B-bar displaying highest strength (with 0.47%Mn and 0.02%S).

Figure 11. Graphite structure in B-bar displaying lowest strength (with 0.47%Mn and 0.13%S).

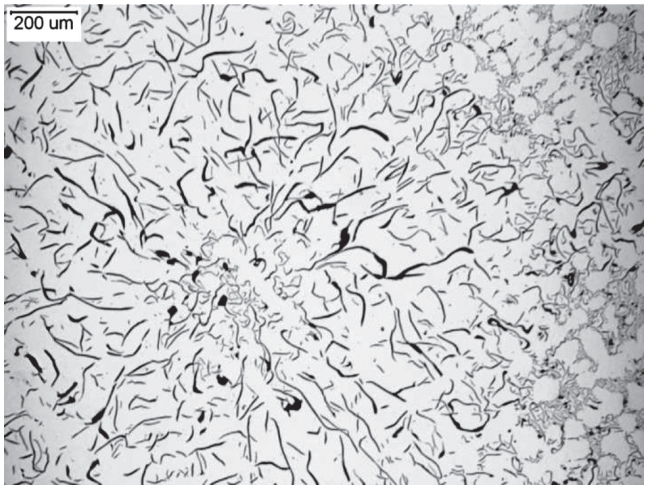

Figure 12. Graphite structure in B-bar displaying highest strength (with 0.78%Mn and 0.02%S).

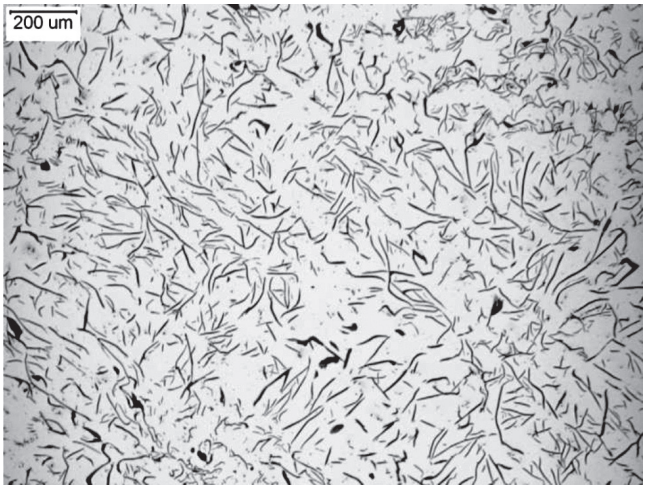

Figure 13. Graphite structure in B-bar displaying lowest strength (with 0.78%Mn and 0.15%S).

Eutectic cell count was performed on selected B test bar specimens to look for trends. The results of the cell count analysis are shown in Figure 14.

Chill Measurements

The W2 chill wedges were broken in two at mid-length according to ASTM Standard A367. The clear chill and total chill widths were measured and the results are listed in Table 4. Total chill width ranged from 3.5 to 7.5 as recorded in 1/32nd inch intervals.

Thermal Analysis

Thermal analysis cups were poured along with the chill wedges from each of the 24 ladles. Various arrests were determined from the cooling curves including the austenite liquidus (Tliq), the eutectic start temperature (TES), the temperature of maximum undercooling (TELow) and the maximum temperature at the eutectic arrest (Teu). The tempera-

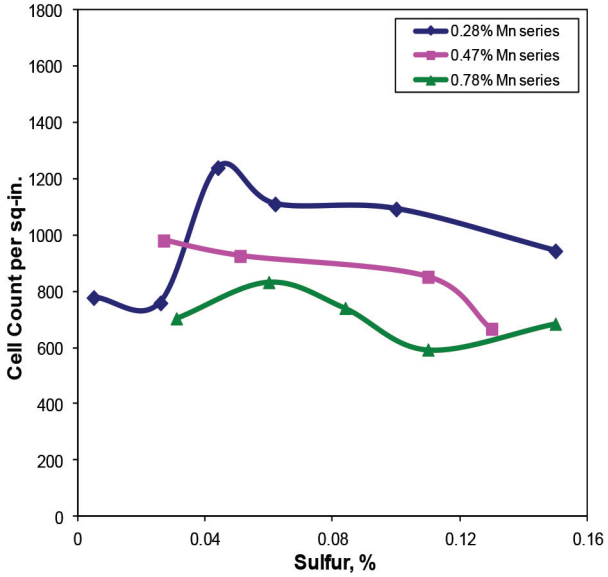

Figure 14. Correlation of eutectic cell count with sulfur in B-bars at three Mn levels.

Table 3. Results of Chill Measurements and Thermal Analysis

Series ID	% Sulfur	Chill Width 1/32nd inch		Thermal Analysis Parameters, deg C				
		Clear	Total	Tliq	TES	TElow	Teu	Teu - TElow
0.28%Mn Series								
	0.005	4.5	7.0	1195.9	1176.6	1143.1	1151.8	8.7
	0.017	3.0	4.0	1196.1	1181.8	1147.8	1152.7	4.9
	0.026	2.5	3.5	1198.3	1180.5	1148.4	1152.9	4.5
	0.044	3.0	4.0	1194.5	1179.7	1145.3	1150.3	5.0
	0.062	3.0	4.5	1192.6	1177.2	1143.9	1150.1	6.2
	0.087	3.0	4.5	1192.0	1174.1	1142.9	1149.5	6.6
	0.10	3.5	4.5	1194.1	1171.3	1142.3	1149.0	6.7
	0.15	3.5	7.5	1195.0	1166.4	1138.7	1144.3	5.6
0.47%Mn Series								
	0.030	3.5	5.0	1200.2	1173.7	1143.7	1144.6	0.9
	0.020	3.0	3.5	1198.0	1177.7	1145.1	1151.0	5.9
	0.027	2.5	4.0	1198.5	1179.5	1145.4	1150.9	5.5
	0.051	3.5	4.5	1197.3	1180.4	1144.1	1145.4	1.3
	0.067	3.5	4.5	1196.4	1178.2	1142.8	1149.1	6.3
	0.085	3.5	5.5	1197.5	1175.6	1142.3	1147.6	5.3
	0.11	2.5	5.0	1197.8	1175.5	1143.1	1147.8	4.7
	0.13	3.0	5.0	1198.1	1175.5	1142.9	1148.1	5.2
0.78%Mn Series								
	0.031	4.5	6.0	1205.7	1173.1	1139.5	1145.0	5.5
	0.026	4.0	6.5	1203.6	1174.9	1141.1	1147.5	6.4
	0.026	4.0	6.0	1204.9	1175.7	1140.8	1143.2	2.4
	0.043	3.5	6.0	1204.7	1179.3	1140.5	1143.6	3.1
	0.060	3.5	5.5	1203.0	1181.7	1140.8	1147.2	6.4
	0.084	3.5	5.5	1205.1	1177.2	1141.3	1146.9	5.6
	0.11	3.5	6.0	1206.6	1175.7	1140.6	1143.9	3.3
	0.15	3.5	6.0	1207.3	--	--	--	--

ture difference between the Teu and the TELow was also calculated. The results of these measurements are shown in Table 3.

Discussion

At all three Mn levels, tensile strength was found to increase and then decrease with increasing sulfur. The correlation of tensile strength with sulfur content for the three Mn levels is shown in Figures 1 to 3. The maximum tensile strength and minimum tensile strength in each bar size and for each Mn series are listed in Table 4 along with the sulfur content at the high and low strength levels. In addition, the ratio of UTS_{max} to UTS_{min} is also listed in Table 4.

Within a given Mn series and bar size, the range in strength between the lowest and highest values ranged from a low of 16% to a high of 71%. The average range in strength was around 8 ksi, independent of section size. Note that these lightly-alloyed Class 35 irons exceeded 40 ksi in the B test bars of the 0.5% and 0.8%Mn series. Furthermore, at an optimum sulfur content, Class 35 iron properties were achieved in the 3 inch bars. The variation in strength with sulfur content observed in this study is consistent with predictions, and the findings in the literature review.[5] Strength correlated best with MnS solubility limit, rather than with stoichiometric balancing of Mn and S.

For comparison, the theoretical solubility limit of sulfur, as well as the excess Mn content at the optimum sulfur concentration in each Mn series, is listed in Table 4. The results show that the optimum sulfur (%S at UTS_{max}) ranged from 0.020% to 0.044%, it decreased with increasing Mn content, and it was consistently below the "theoretical" (calculated) solubility limit of MnS. In contrast, the excess Mn content at the maximum strength decreased with increasing Mn concentration. The excess %Mn increased from 0.21% to 0.74% as Mn increased from 0.28% to 0.78% when maximum strength was achieved. Furthermore, in the 0.78%Mn series, when an excess Mn of 0.3% (0.15%S) was reached, tensile strengths in all four sections reached their lowest values.

Statistical analysis was performed on some of the data for the A and B test bars to verify that the observed trends in strength are statistically significant. Tensile strength data for all three Mn series were plotted in the manner shown in Figure 15. Each point in the graph represents the average tensile strength pulled from a certain bar size and with specified sulfur content. The error bar represents the "control limit" of the experiment which indicates 95% probability of significant difference in the data, if it is outside the error bar. The "control limit" takes into account the experimental and measurement errors as well as the degree of freedom, or the sulfur levels in this case. A trend of increasing, then decreasing tensile strength as a function of sulfur was observed throughout. The tensile strength

Table 4. Correlation of Tensile Properties and Sulfur Content

Series ID	Bar	UTS min	%S	UTS max	%S	Ratio of Max:Min	Mn x S @ UTSmax	Theoretical Solubility Limit (Mn x S = 0.03)	Excess Mn (Mn – 1.7x S)
0.28% Mn	A	26.5	0.15	45.2	0.044	1.71	0.012	0.11%S	0.21
	B	26.8	0.15	38.6	0.044	1.44	0.012		0.21
	C	25.8	0.15	33.9	0.026	1.31			
	3”	28.4	0.15	33.5	0.044	1.18			
0.47% Mn	A	40.9	0.11	48.4	0.030	1.18	0.014	0.064%S	0.42
	B	33.4	0.13	40.6	0.030	1.16	0.014		0.42
	C	26.2	0.13	35.1	0.027	1.34			
	3”	25.7	0.11	35.4	0.027	1.38			
0.78% Mn	A	40.9	0.08	49.6	0.026	1.21	0.020	0.038%S	0.74
	B	33.4	0.15	42.0	0.026	1.26	0.020		0.74
	C	29.5	0.11	37.1	0.026	1.26			
	3”	28.5	0.10	36.0	0.043	1.26			

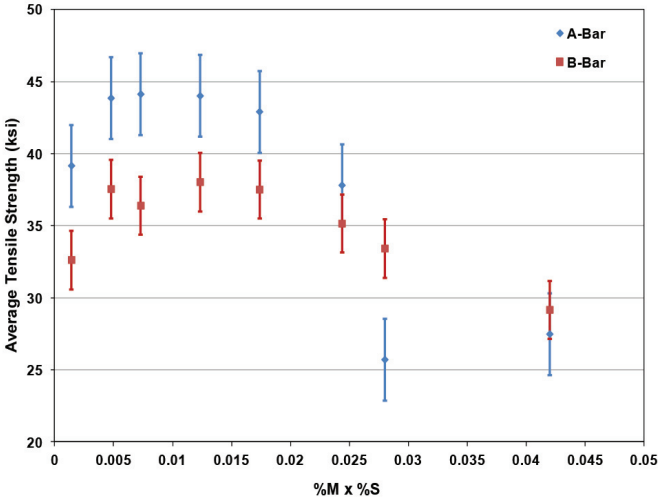

Figure 15. Mean and range in tensile strengths in the A and B bars as a function of %Mn times %S at a 0.28%Mn level.

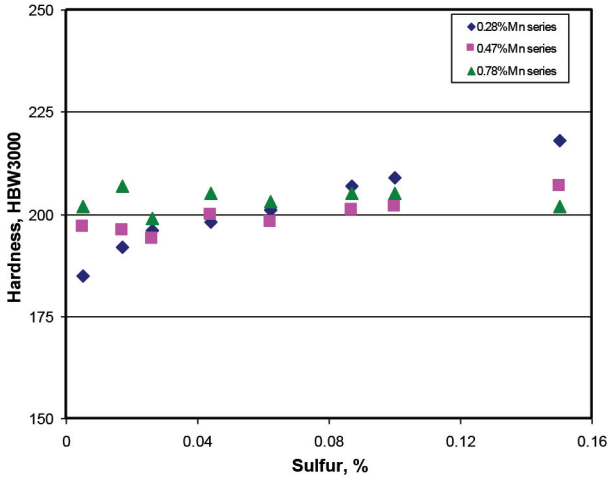

Figure 16. Hardness in B-bars as a function of sulfur content at three Mn levels.

reaches a maximum at 0.03% sulfur and starts to decrease around 0.1% sulfur. The effect of sulfur on tensile strength is also more pronounced in the smaller A test bar than the larger B test bar, but it is less significant with increasing Mn content.

The maximum attainable strength increased with increasing Mn concentration. The increase in strength with Mn was consistent in all four cast section sizes. The increase in Mn content was accompanied by a steady and modest decrease in carbon equivalent due to some carbon loss over time. The carbon equivalent value ranged from a high of 4.03 in the 0.28%Mn series to a low of 3.83 in the 0.78%Mn series, as shown in Table 1. The increase in strength with increasing Mn content was largely attributed to the decrease in carbon equivalent value and its influence on strength.

Hardness

Hardness was generally unchanged with increasing sulfur content in the two series containing higher Mn levels, as shown in Figure 16. In contrast, hardness increased continuously with sulfur content for the B bars of the 0.28%Mn series. Hardness increased from 185 to 218 HB, which is an 18% increase in hardness with no change in pearlite content; all samples were 100% pearlitic.

The increase in hardness with sulfur content in the low-Mn alloy series is attributed to the influence of free sulfur on pearlite transformation and combined carbon content. At higher levels, sulfur is known to increase hardness, based on past research.[7,8] The influence of sulfur on hardness was attributed to the concentration of sulfur at the graphite-metal interface. At the very highest level, some intercellular carbides were present and they further increased hardness.

For the alloys with higher Mn levels, hardness was relatively unchanged. It is surmised that at higher Mn levels, MnS precipitation occurs and the soluble, or free sulfur content is restricted to lower values.

The ratio of tensile strength to Brinell hardness has long been used to indicate the quality of the flake graphite structure.[9] The relationship between UTS/HB ratio and microstructure shown in Table 5 was proposed by Barlow and Lorig.[10] As the flake graphite structure becomes more refined, the UTS/HB ratio increases. In Figure 17 the UTS/HB ratio is correlated with sulfur content for the 0.28%, 0.47% and 0.78%Mn series. The UTS/HB ratio shows a slight rise in value and then a significant decrease in value with increasing sulfur content.

The decrease in UTS/HB ratio strongly suggests that a change in the graphite structure is occurring with increasing sulfur content. Graphite flake size was determined for most of the samples; the mean and maximum flake sizes are plotted as a function of sulfur content in Figures 18 and 19. Mean flake size appears to converge from a wider distribution at low sulfur levels to a narrower distribution at higher sulfur levels. There was no correlation of maximum flake size with sulfur content as shown in Figure 19.

The range in strength among the four bar sizes varied depending on the sulfur content. The range was greatest at the optimum sulfur level where UTSmax occurred, as shown in Figures 1 to 3. The range in strength was lowest at the highest concentration of sulfur. This finding suggests that the negative effect of sulfur on graphite structure is greatest in the lighter cast sections, where solidification rates are highest.

Composition and Chill Width

Clear chill and total chill were measured in the W2 chill wedge. Within each of the three Mn series, chilling tendency first decreased and then increased with increasing sulfur. The greatest variation in chilling tendency was observed in the 0.28%Mn series. The correlation between

Table 5. Relationship between Strength-to-Hardness Ratio and Graphite Structure[10]

Carbon Equivalent	Ratio UTS/HB	Microstructure
3.45 - 3.65	210 and over	Smallest cell, normal graphite
	190 – 210	Small cell, normal graphite
	180 – 190	Medium cell, some type D graphite
	170 – 180	Large cell, some type D graphite
		Medium cell, completely type D graphite
	160 – 170	Large cell, partial type D graphite
	160 and below	Large cell, completely type D graphite
3.65 – 3.85	190 – 210	Small cell, normal graphite
	180 – 190	Medium cell, normal graphite
		Small cell, partial type D graphite
	170 – 180	Large to medium cell, with partial type D graphite
	160 – 170	Large cell, type D graphite or free ferrite
3.85 – 4.20	190 – 210	Medium cell, normal graphite
	180 – 190	Medium cell, large normal graphite
	170 – 180	Medium or large cell, some type D graphite
	160 – 170	Large cell, type D graphite
	160 and below	Free ferrite, type D graphite

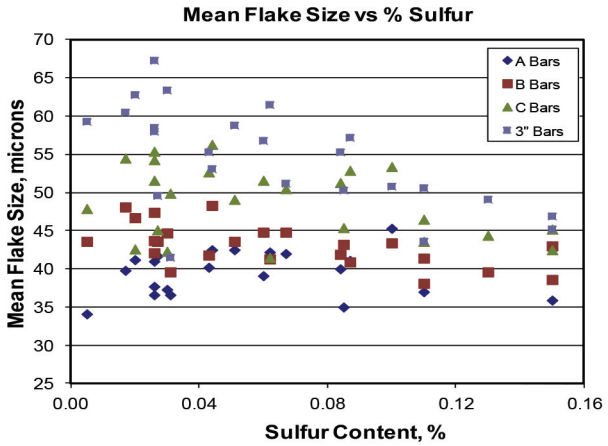

Figure 18. Mean flake size as a function of sulfur content and bar size.

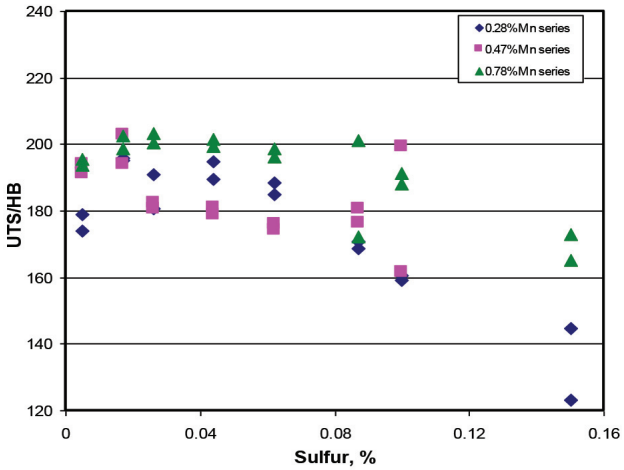

Figure 17. UTS/HB ratio in the B bars as a function of sulfur content at three manganese levels.

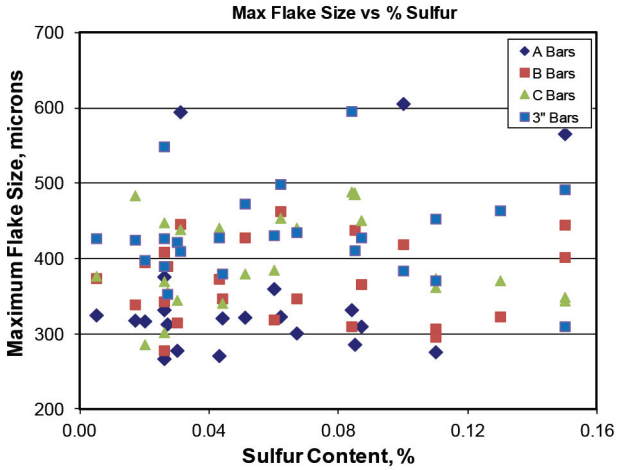

Figure 19. Maximum flake size as a function of sulfur content and bar size.

clear chill, total chill and sulfur content is shown in Figure 20. Only the lowest and highest sulfur contents produced high chilling tendencies. At the sulfur levels that yielded the highest strength, chilling tendency was moderate.

Thermal analysis data is often used to predict chilling tendency in cast iron, and a strong correlation between total chill and the TElow temperature is generally seen. Figure 21 shows a good correlation between total chill and TElow temperature for the 24 chill wedges poured in this investigation.

The TElow temperature tended to increase and then decrease with increasing sulfur concentration in all three Mn series, as shown in Figure 22. In the 0.28%Mn series, following an initial rise in temperature, TELow decreased continuously, producing a wide range in TELow values. The continuous decrease in TELow temperature with increasing sulfur is attributed to the negative influence of sulfur on the growth of graphite.

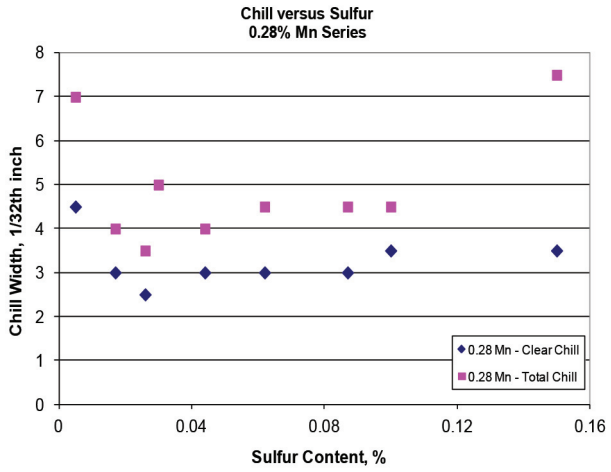

Figure 20. Chill width as a function of sulfur in W2 chill wedges in the 0.28% Mn series.

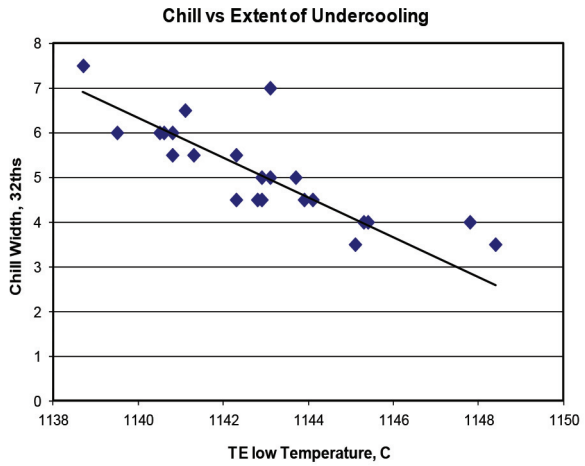

Figure 21. Chill width as a function of TElow temperature in W2 chill wedges.

For the 0.47% and 0.78%Mn series, a second inflection in the curve occurred at a higher sulfur level, and the range in TELow values was much reduced. The second inflection that occurred at the intermediate S concentrations has been attributed to coarsening of the MnS inclusions and their influence on nucleation of the eutectic cells.

A general shift in TElow values to lower temperatures was also observed for each Mn series in Figure 22, and the shift is attributed to the influence of Mn on the equilibrium eutectic temperature.

When looking at the 1st derivative of the thermal analysis cooling curve, the eutectic start (TES) temperature is detected by a change in the slope of the cooling curve in the region between the austenite liquidus and the temperature of maximum undercooling (TElow temperature). The TES temperature was derived from the thermal analysis curve, and the correlation of TES temperature with sulfur content is shown in Figure 23.

As with the TElow temperature, the TES temperature first increased and then decreased with increasing sulfur concentration. In the 0.28%Mn series, following an initial rise in temperature, TES temperature decreased continuously with increasing sulfur. The continuous decrease in TES temperature with increasing sulfur is attributed to the influence of sulfur on the nucleation of graphite. Based on the literature review, sulfur promotes undercooling by lowering the surface tension, or surface energy associated with the graphite-liquid metal interface. For the 0.47% and 0.78%Mn series, a second inflection in the curve occurred at a higher sulfur level, and the TES temperature tended to level off, see Figure 23. The second inflection that occurred in the higher Mn alloys is attributed to the influence of Mn on controlling the free, or soluble sulfur concentration in the melt at the time of graphite nucleation, and by the coarsening of the MnS inclusions which favor graphite nucleation.

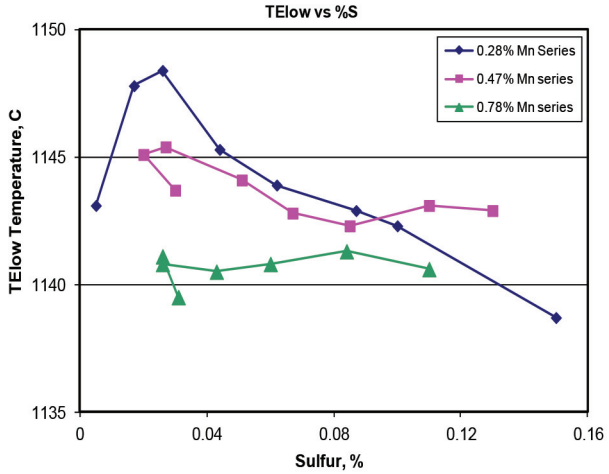

Figure 22. Temperature of maximum undercooling (TELow) as a function of sulfur at three Mn levels.

Cell Count

Cell count did not vary significantly at intermediate to high sulfur contents, as shown in Figure 14. However, cell count was reduced at the lowest sulfur contents in the 0.28% Mn series. This finding is consistent with the investigation performed by Muzumdar and Wallace,[11] as shown in Figure 24 for alloys containing 0.75%Mn, where cell count quickly rose to a maximum at 0.04%S and remained relatively unchanged at levels up to 0.12%S. In the current study, there was a modest shift to lower cell counts with increasing manganese content. At higher Mn levels, the soluble or free sulfur is lower, and the reduced cell count is attributed to a low free sulfur content.

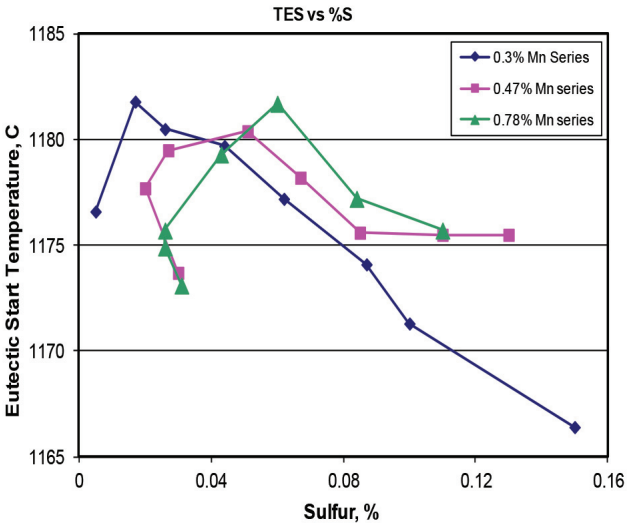

Figure 23. Eutectic start temperature (TES) as a function of sulfur content at three Mn levels.

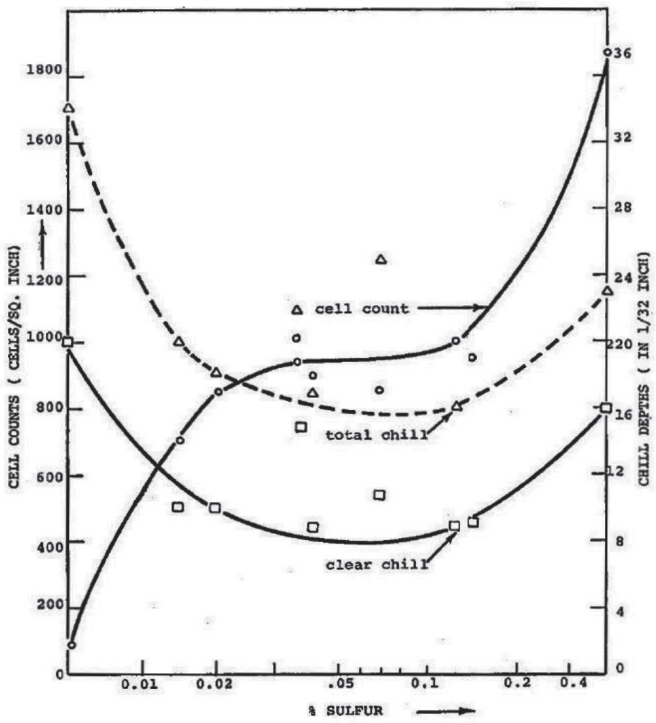

Figure 24. Cell count and chill depth as a function of sulfur in 0.75%Mn cast iron, after Muzumdar and Wallace[11].

MnS Inclusions

The distribution of the MnS inclusions varied from a concentration of MnS inclusions in interdendritic regions to a random distribution of MnS inclusions. Those alloys with lower sulfur contents displayed an interdendritic distribution, whereas in those alloys with higher sulfur contents, the MnS inclusions were more uniformly distributed. The two types of MnS distributions are attributed to whether the onset of MnS precipitation occurred above or below the austenite liquidus temperature. When MnS precipitation precedes primary austenite dendrite formation, that is, when %Mn x %S is high (>0.03) and the solubility limit of MnS is exceeded, the MnS inclusions are more randomly distributed.

Spiky Graphite and Carbides

Spiky graphite was visible in all three Mn series. It generally occurred at sulfur levels above 0.08%, and in all section sizes. Trace levels were seen in a few sections at levels as low as 0.067%S.

Intercellular carbides were visible at the highest sulfur levels, but only in the 0.28%Mn series. At higher Mn levels, carbides were not visible, even at sulfur levels up to 0.15%. When intercellular carbides first appeared, they were associated with phosphide eutectic. As sulfur increased, the carbides became the predominant intercellular phase, as shown in Figure 5. For comparison, note that Alderson[7] observed spiky graphite and intercellular carbides in B bars containing 0.12%S and 0.08%Mn.

The free sulfur content was calculated based on the solubility limit of MnS at the eutectic temperature (nominally 1150°C [2102°F]). Using Gibbs free energy of formation for MnS and published interaction coefficients for C, Si and Mn on the activity of S in iron, thermodynamic calculations[12] were performed to determine the solubility limit of MnS in the cast iron alloys of this study. The theoretical solubility limit occurs when %Mn x %S = 0.03. Free sulfur is calculated by assuming that MnS precipitated in the melt until equilibrium solubility was met. Figure 25 illustrates the method used to determine free sulfur content in the 0.78%Mn-0.15%S alloy.

The correlation of free sulfur and total sulfur for the three Mn series is shown in Figure 26. At lower sulfur levels, sulfur is fully soluble. When the MnS solubility limit is exceeded, there is an inflection in the free sulfur vs. total sulfur curve. In the 0.28% Mn series, MnS solubility is high and the free sulfur vs. total sulfur curve is linear up to high sulfur concentrations. However, at higher Mn lev-

els, free sulfur is restricted by Mn to lower concentrations. Manganese buffers the free sulfur content, limiting it to a narrow range at most total sulfur contents (above the MnS solubility limit).

Based on the microstructural examinations of the 0.28% Mn series, intercellular carbides were first observed at a sulfur concentration of 0.10%. For the 0.78% Mn series at a total sulfur level of 0.15%, the free sulfur concentration is only 0.049%. Since the free sulfur contents in the 0.47% Mn and the 0.78% Mn series were held to lower levels (below nominally 0.10%S) as shown in Figure 26, no carbides are expected and, indeed, none were observed. This finding suggests that, when holding free sulfur to a maximum value of 0.10%, intercellular carbides will be prevented.

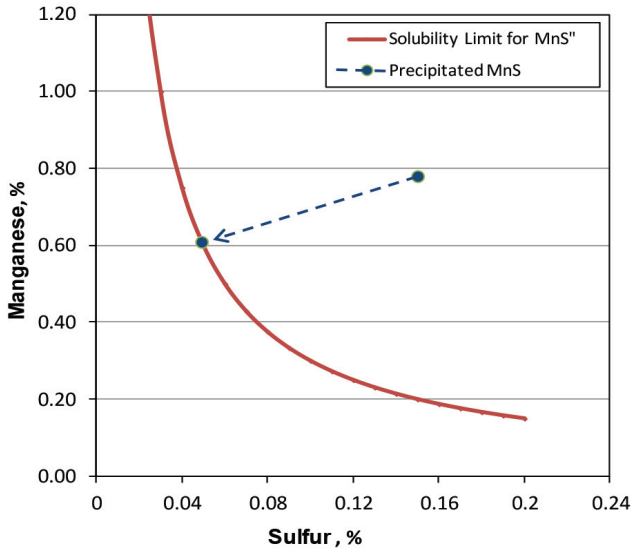

Figure 25. Calculation of free sulfur (0.049%) at the eutectic solidification temperature (1150C) for an alloy containing 0.78% Mn and 0.15%S.

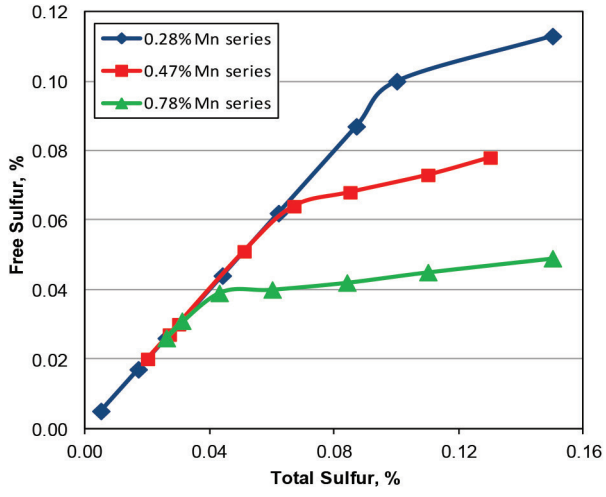

Figure 26. Calculation of free sulfur as a function of total sulfur at the eutectic solidification temperature (1150C) and at the three Mn levels in this study.

Preferred Mn and S Concentrations

Based on the literature review in Part I and the experimental work in Part III, it is possible to obtain higher strengths than generally thought possible in gray cast irons. The experimental work shows that at optimum levels of Mn and S, the strength can be 6 to 10 ksi higher than in poorly balanced chemistries for Class 35 irons cast in sections up to 3 inches. The highest strengths were attained at sulfur levels well below that commonly recommended.

The findings indicate that balancing according to the solubility limit of MnS will produce the highest strengths in gray cast iron. The optimum balance between Mn and S and strength in the B bars of this study is shown in Figure 27. The optimum combinations of Mn and S occurred in chemistries below the theoretical solubility limit of manganese sulfide.

When balanced according to the solubility limit of MnS, the sulfur levels are relatively low and the manganese levels are generally higher than proposed by stoichiometric balancing. For example, with a 0.78%Mn level, the optimum sulfur concentration was 0.02%, yielding an excess Mn content of 0.74%.

The findings also show that certain levels of Mn and S are undesirable from the point of view of spiky graphite and intercellular carbide formation. To avoid spiky graphite and intercellular carbides, it is proposed that the proper way to balance S with Mn is to control the free sulfur content, rather than control the excess Mn content [where excess Mn = (%Mn) - 1.7*(%S)]. In order to avoid spiky graphite, an upper limit of 0.08% free sulfur is recommended.

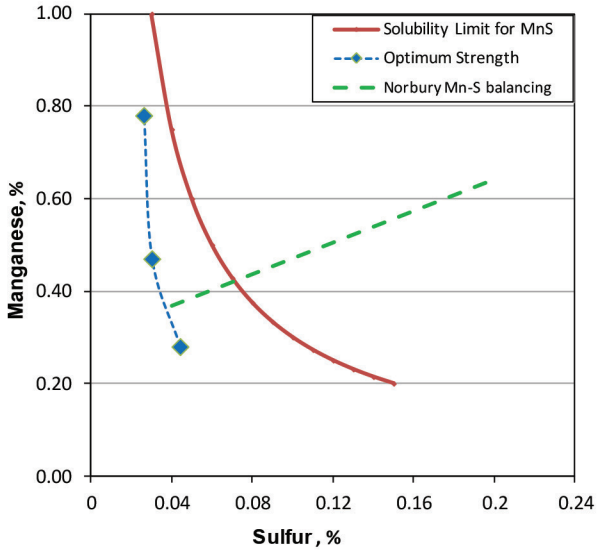

Figure 27. Mn and S levels at maximum strength compared with the theoretical solubility limit of MnS at the eutectic solidification temperature (1150C), and with stoichiometric balancing with 0.30% excess Mn as proposed by Norbury.[1]

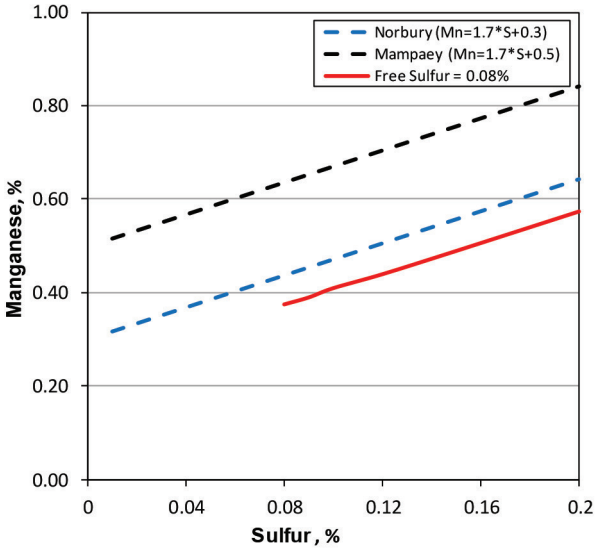

Figure 28. Graphical presentation of optimum balancing of Mn and S for limits with regard to forming carbides and spiky graphite.

Compositions with free sulfur contents of 0.08% were calculated and are plotted as a function of Mn and total S in Figure 28. For comparison, two common methods of stoichiometric balancing of Mn with S with an excess manganese of 0.3% (proposed by Norbury[1]) and 0.5% (proposed by Mampaey[2]) are shown as well. The application of stoichiometric balancing to avoid degenerate graphite and intercellular carbides is quite similar to balancing according to a free sulfur content of 0.08%.

Conclusions

The variations in strength and composition that were observed in this study are consistent with predictions, based on the findings in the literature review. The following conclusions were made:

1. The experimental work with a Class 35B cast iron chemistry, shows that at optimum levels of Mn and S, tensile strength can be 6 to 10 ksi higher than at poorly balanced levels.
2. Strengths reached 42 ksi in the 1.2 inch B test bar, and 36 ksi in the 3 inch bar. For each Mn series, the differences in strength between maximum and minimum values were 44% and 38% for the B bars and 3 inch bars, respectively.
3. Tensile strength was maximized when Mn and S were balanced according to the solubility limit of MnS. The solubility limit occurs when the value of %Mn x %S equals nominally 0.03. Tensile strength decreased when combinations of Mn and S exceeded the solubility limit of MnS at the eutectic temperature.
4. Balancing by stoichiometric methods with an excess of 0.30% Mn produced much lower strength, particularly at higher Mn levels.
5. Intercellular carbides were observed at levels of 0.10% S and above in the 0.28%Mn series. At higher Mn levels, no carbides were seen. Mn controlled free S, and intercellular carbides were avoided when free sulfur was held below 0.10%.
6. Spiky graphite was observed in all cast sections and Mn levels at higher sulfur concentrations. Spiky graphite was generally avoided when free sulfur was held below 0.08%.
7. Manganese concentrations that produce a free sulfur of 0.08% are very similar to those that produce an excess Mn of 0.3%, when applying stoichiometric balancing. However, such sulfur levels are well above those that produce maximum strength.
8. The tensile strength-to-hardness ratio varied with composition and decreased with increasing sulfur content. The fall in UTS/HB ratio indicates that the decrease in strength accompanied a change in graphite structure.
9. Plots of the eutectic start temperature (TES) with sulfur content displayed an inflection at intermediate sulfur contents. The inflection coincided with the formation of MnS inclusions at the time of graphite nucleation. It also coincided with a rapid decrease in strength with increasing sulfur.
10. The change in the TES temperature provides a hint as to the effect of Mn and S on the variation in strength of cast iron. The increase and then decrease of TES clearly indicate the effect of Mn and S on graphite nucleation. Prior and after the inflection point, sulfur aids and then hinders strength. The inflection point is a function of Mn as well.
11. Controlling the sulfur content is therefore paramount to maximizing the strength in gray cast iron. This research shows that Mn is only effective up to the solubility limit. Further research is needed to better understand the negative effects of sulfur at concentrations beyond the solubility limit of MnS.

Acknowledgments

This research was funded by American Foundry Society under Research Contract Project 12-13#04 Influence of Mn & S on the Properties of Cast Iron. The authors are very grateful for the financial support of AFS and for the encouragement and support of the AFS 5R Committee members.

REFERENCES

1. Norbury, A.L. “Manganese in Cast Iron,” BCIRA Bureau Report 53, Third Int’l Foundry Congress, London (1929).
2. Mampaey, F. “The manganese:sulfur ratio in gray irons,” Fonderie Belge – De Belgische Gieterej, , vol. 51, no. 1, pp. 11-25 (March 1981).
3. “The Effects of Alloying Elements in Cast Iron – 2: Sulfur,” BCIRA Report 1229, pp. 271-276 (May, 1976).

4. "The Effects of Alloying Elements in Cast Iron – 4: Manganese," BCIRA Report 1245, p. 570 (November, 1976).
5. Gundlach, R.B., "Influence of Mn and S on the Properties of Cast Iron: Part I – Historical Perspective," *AFS Transactions,* vol. 122, pp. 287-303 (2014).
6. Meyer, M.H., Gundlach, R.B., Williams, D.C., Winardi, L., "Influence of Mn and S on the Properties of Cast Iron Part II – Experimental Design: Aspects of Melting and Pouring," *AFS Transactions*, vol. 122, pp. 273-278 (2014).
7. Alderson, A., "The Influence of Manganese and Sulfur on the Structure and Mechanical Properties of Grey Cast Iron," *BCIRA J*., pp. 59-67 (1983).
8. Collaud, A., Thieme, J.C., "Toughness of Flake-graphite Cast Iron as an Index of Quality, and New Methods for Improving the Toughness," *Foundry Trade Journal*, pp. 315-316 (March 16, 1957).
9. "Iron Castings Engineering Handbook," American Foundry Society (2003).
10. Barlow, T.E., Lorig, C.H., "Gray Cast Iron Tensile Strength, Brinell Hardness and Composition Relationships," *AFS Transactions*, vol. 54, p. 545 (1946).
11. Muzumdar, K.M., Wallace, J.F., "Inoculation-Sulfur Relationship in Cast Iron," *AFS Transactions*, vol. 80, p. 317 (1972).
12. Pehlke, R.D., Gundlach, R.B., Unpublished research.